Induced-fit process through mechanical pivoting of aromatic walls in host-guest chemistry of calix[6]arene aza-cryptands

Andrea Brugnara[a], Luca Fusaro[b], Michel Luhmer[b], Thierry Prangé[c], Benoit Colasson*[a] and Olivia Reinaud*[a]

[a] Laboratoire de Chimie et de Biochimie Pharmacologiques et Toxicologiques (CNRS UMR 8601), Université Paris Descartes, 45 rue des Saints-Pères, 75006 Paris, France.
[b] Laboratoire de Résonance Magnétique Nucléaire Haute Résolution, Université Libre de Bruxelles, Avenue F.D. Roosevelt 50, CP160/08, B-1050 Brussels, Belgium.
[c] Laboratoire de Cristallographie et de Résonance Magnétique Nucléaire Biologiques (CNRS UMR 8015), Université Paris Descartes, 4, Avenue de l'Observatoire, 75006 Paris, France.

Table of contents

General experimental methods.

CH_2Cl_2 was dried over CaH_2 and distilled under argon atmosphere; THF was dried over Na/benzophenone and distilled under argon atmosphere. Other solvents and chemicals were of reagent grade and were used without further purification. **^{1}H** and **^{13}C NMR** spectra were recorded on a Brucker ARX (250 MHz) spectrometer or an Advance 500 spectrometer (500 MHz). Chemical shifts are expressed in ppm. **MS (ESI)** analyses were obtained with a ThermoFinnigen LCQ Advantage spectrometer using methanol as solvent. **HRMS** and **Elemental Analysis** were performed at the "Institut de Chimie des Substances Naturelles", Gif-sur-Yvette, France. **IR** spectra were obtained with a Perkin-Elmer Spectrum on FTIR spectrometer equipped with a MIRacleTM single reflection horizontal ATR unit (germanium crystal). XRD diffraction data were recorded at the European Synchrotron Facility (ESRF, Grenoble), beam line BM30A (FIP). The wavelength was set to 0.865 Å and the detector was an ADSC Quantum 315r. The temperature of the crystal was maintained at 100 K during data collection.

✱ Synthesis of $[Cu^I3]PF_6$

$Cu(CH_3CN)_4PF_6$ (1.2 mg, $3.2\cdot10^{-3}$ mmol) was added to a solution of **3** (4.2 mg, $3.2\cdot10^{-3}$ mmol) in 0.6 mL of outgassed acetonitrile, and the system was stirred under Argon atmosphere. After 1h the solvent was removed under reduced pressure in order to obtain a greenish-yellow solid.

Yield: 97% (4.6 mg, 3.1 10^{-2} mmol).
^{1}H NMR: See Figure S21

✱ Synthesis of $[Cu^{II}3](ClO_4)_2$

A solution of **$Cu(ClO_4)_2\cdot6H_2O$** (0.96 mg, $2.6\cdot10^{-3}$ mmol) dissolved in 50µL of distilled THF was added to a solution of **3** (3.3 mg, $2.6\cdot10^{-3}$ mmol) in 100µL of acetone, and the system was stirred overnight. The organic phase was isolated by centrifugation and the solvent was removed under reduced pressure in order to obtain a green solid.

Yield: 96% (3.8 mg, 2.5 10^{-2} mmol).
UV-Vis in acetone: λ_{max}=720nm (ε= 116 M^{-1} cm^{-1}), See Figure S14.

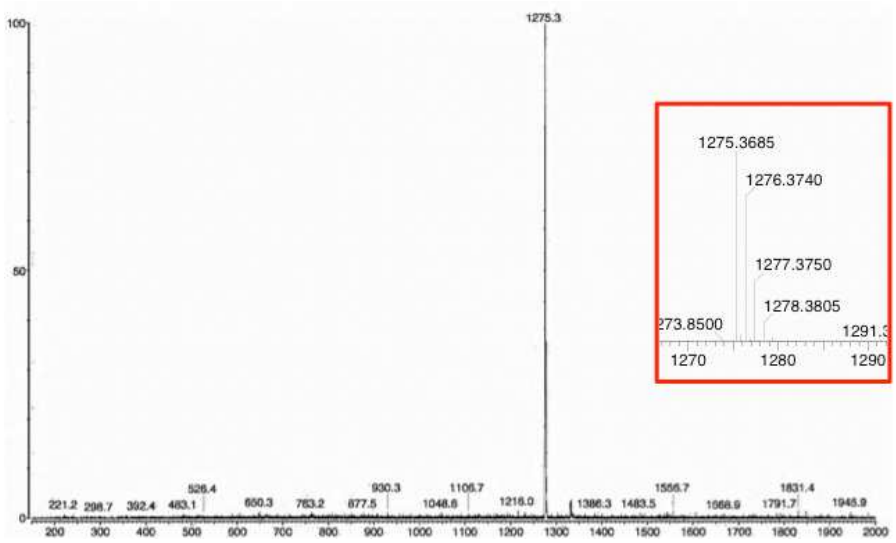

Figure S1: ESMS and HRMS of [**3**·H^+,NO_3] (MeOH).

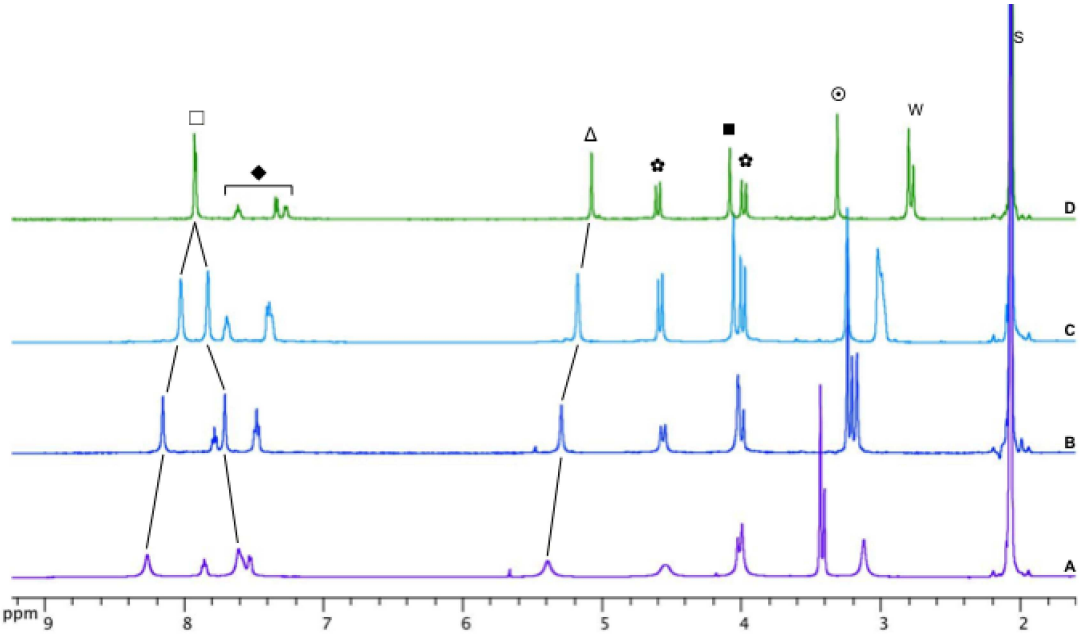

Figure S2: ^{1}H NMR (500 MHz, acetone-d^6) of **3**: A) 240K; B) 260K; C) 280K; D) 300K. □=H_{Ar}, ◆=H_{Py}, w=water, ◘=OCH_2, ■=NCH_2, ✿=$ArCH_2$, ⊙=OCH_3, S=solvent.

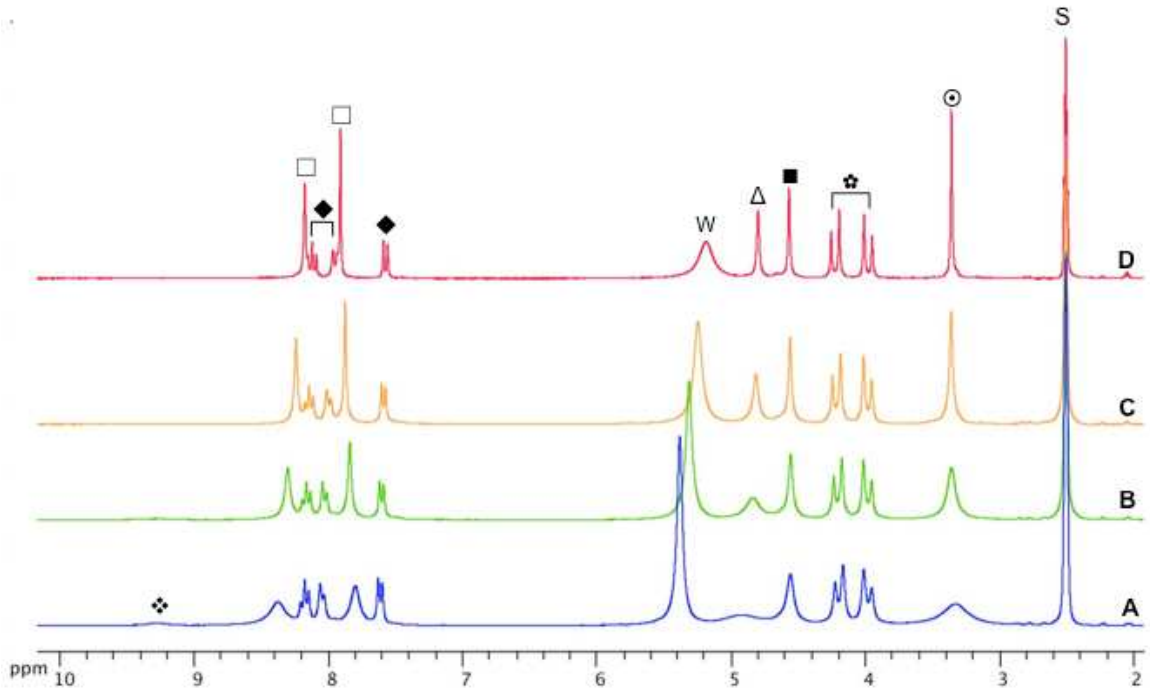

Figure S3: ^{1}H NMR (250 MHz, dmso-d^6) of [**3**·**H**$^{+}$,**NO$_3$**]: A) 300K; B) 320K; C) 340K; D) 360K. ❖=NH^{+}, □=H$_{Ar}$, ◆=H$_{Py}$, w=water, Δ=OCH$_2$, ■=NCH$_2$, ✿=ArCH$_2$, ⊙=OCH$_3$, S=solvent.

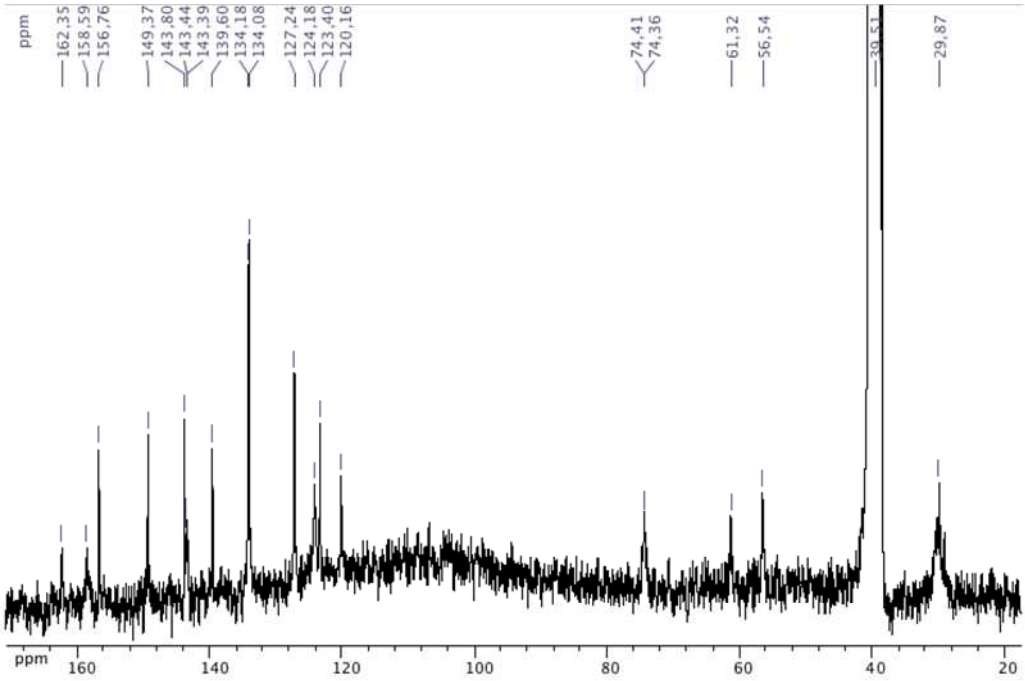

Figure S4: ^{13}C NMR (62.5 MHz, 300K, dmso-d^6) of [**3**·**H**$^{+}$,**NO$_3$**].

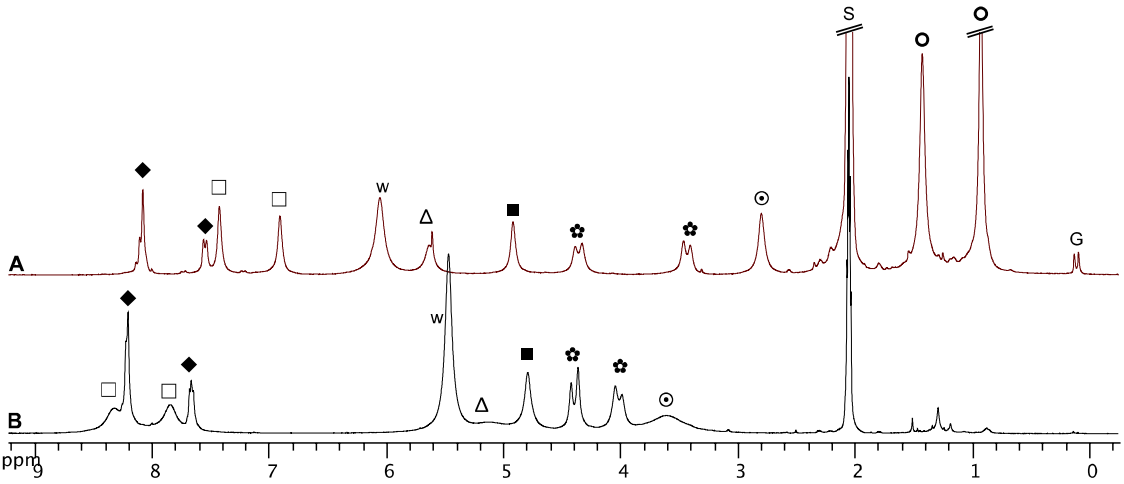

Figure S5: ^{1}H NMR (250 MHz, acetone-d^6, 300K) of: A) **1** in the presence of HNO_3 (10 equivalents); B) **[3·H$^+$,NO$_3$]**. ❖=NH^+, □=H_{Ar}, ◆=H_{Py}, w=water, Δ=OCH_2, ■=NCH_2, ✿=$ArCH_2$, ⊙=OCH_3, S=solvent, O⊨=*t*Bu, G=grease.

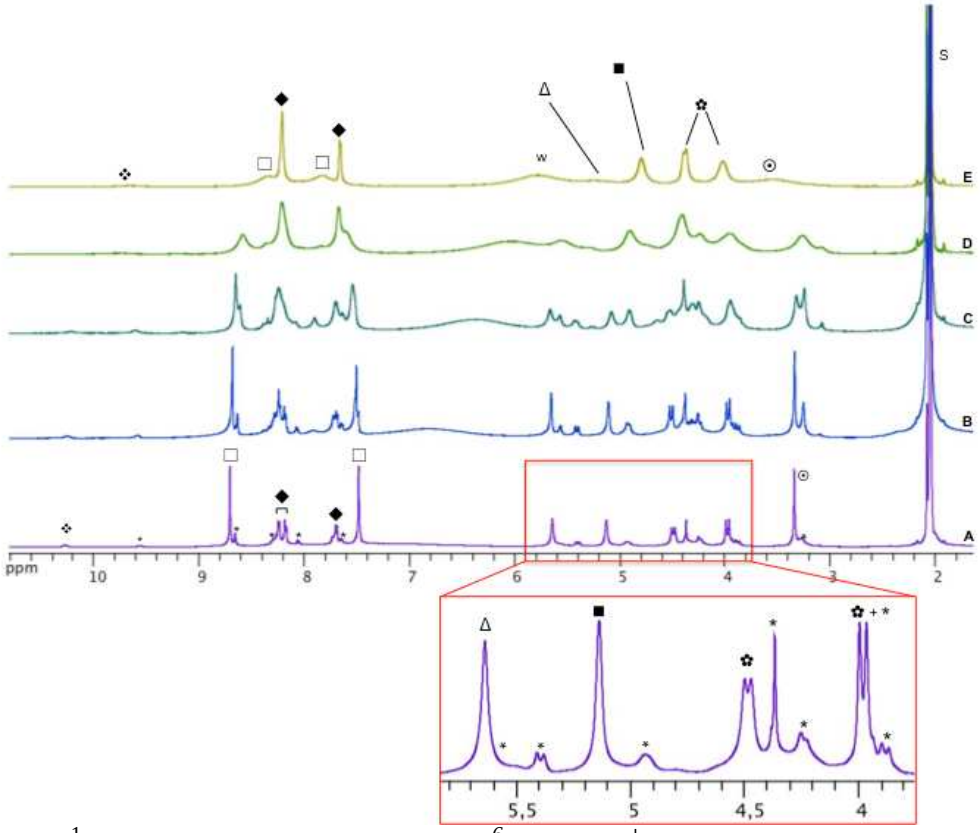

Figure S6: ^{1}H NMR (500 MHz, acetone-d^6) of **[3·H$^+$,NO$_3$]**: A) 220K; B) 240K; C) 260K; D) 280K; E) 300K. ❖=NH^+, □=H_{Ar}, ◆=H_{Py}, w=water, Δ=OCH_2, ■=NCH_2, ✿=$ArCH_2$, ⊙=OCH_3, S=solvent.

NMR characterization of [3·H$^+$,NO$_3$].

A sample of **[3·H$^+$,NO$_3$]** was dissolved in acetone-d_6 (about 5 mg/mL) and transferred into a 5 mm NMR tube equipped with a J. Young valve. The NMR spectra were recorded without sample spinning on a Varian *(part of Agilent)* VNMRS spectrometer operating at 14.1 T (599.94 MHz for ^{1}H and 150.87 MHz for ^{13}C) using either a standard 5 mm triple inverse probe (down to -35°C) or a standard 5 mm broad-band probe (for T < -35°C), both equipped with z-gradient and sample temperature regulation. The signal of the solvent was used for chemical shift referencing (δ ^{1}H = 2.08 ppm, δ ^{13}C = 29.8 ppm).

Variable temperature ^{1}H NMR spectra of this freshly prepared sample are shown in Figure S7. At -35°C, three broadened signals of low intensity were detected at δ > 9 ppm (inset of Figure S7c) and could be assigned to the NH$^+$ group of distinct conformations. Indeed, (i) COSY correlations with the vicinal methylene groups of the TMPA cap were observed for the two most intense signals at 10.6 and 9.6 ppm (see Figure S8), (ii) each signal is involved in EXSY correlations with the other two (Figure S9) and (iii) none of them was observed three weeks later as a consequence of H→D exchange with acetone-d_6 (the impurity signal at 10.0 ppm was still observed; not shown). The signal of water at about 5 ppm is strongly broadened and was efficiently suppressed by T_2-filtering (Figure S7d).

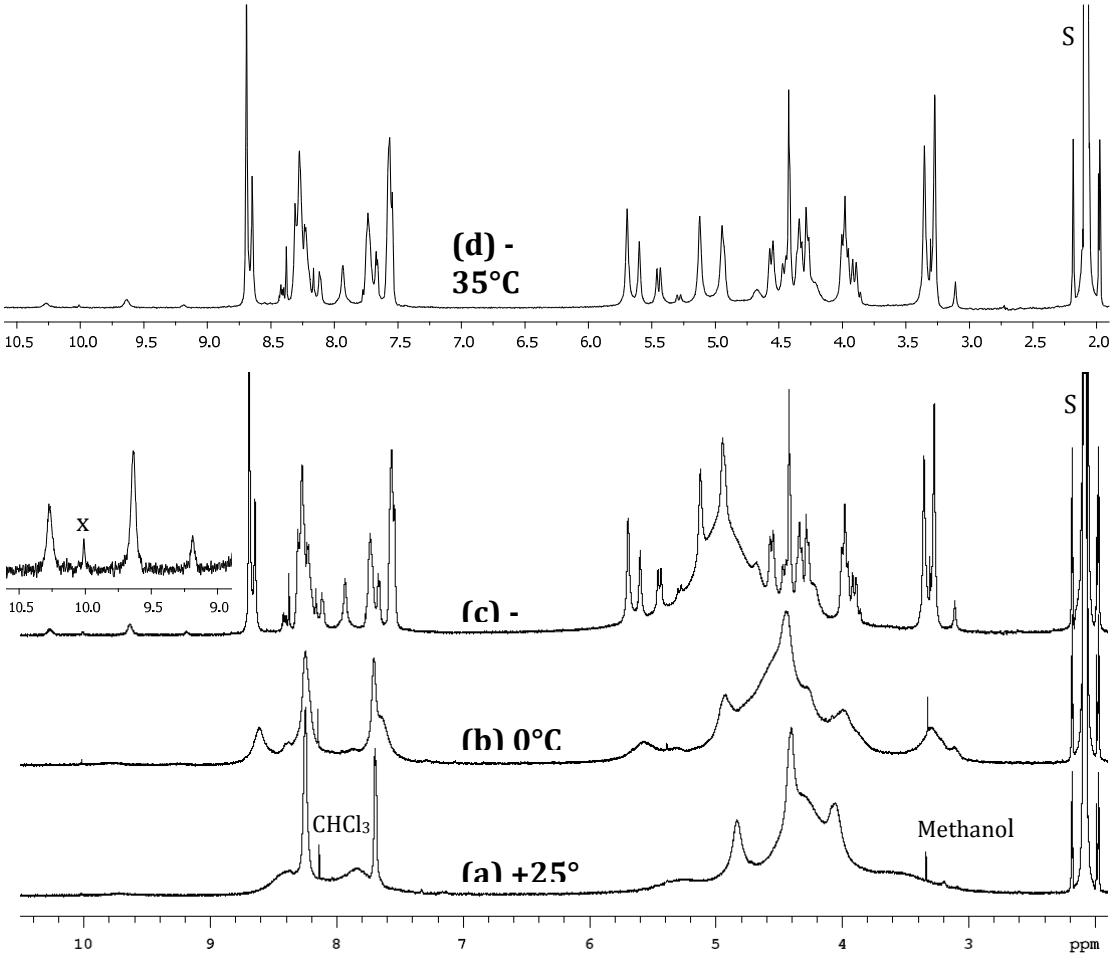

Figure S7: Variable temperature ^{1}H NMR spectra of a freshly prepared sample of **[3·H^{+},NO$_3$]** (a-c) and spectrum recorded at -35°C using a T_2-filter of 4 ms (600 MHz, acetone-d_6). S=solvent, x=impurity.

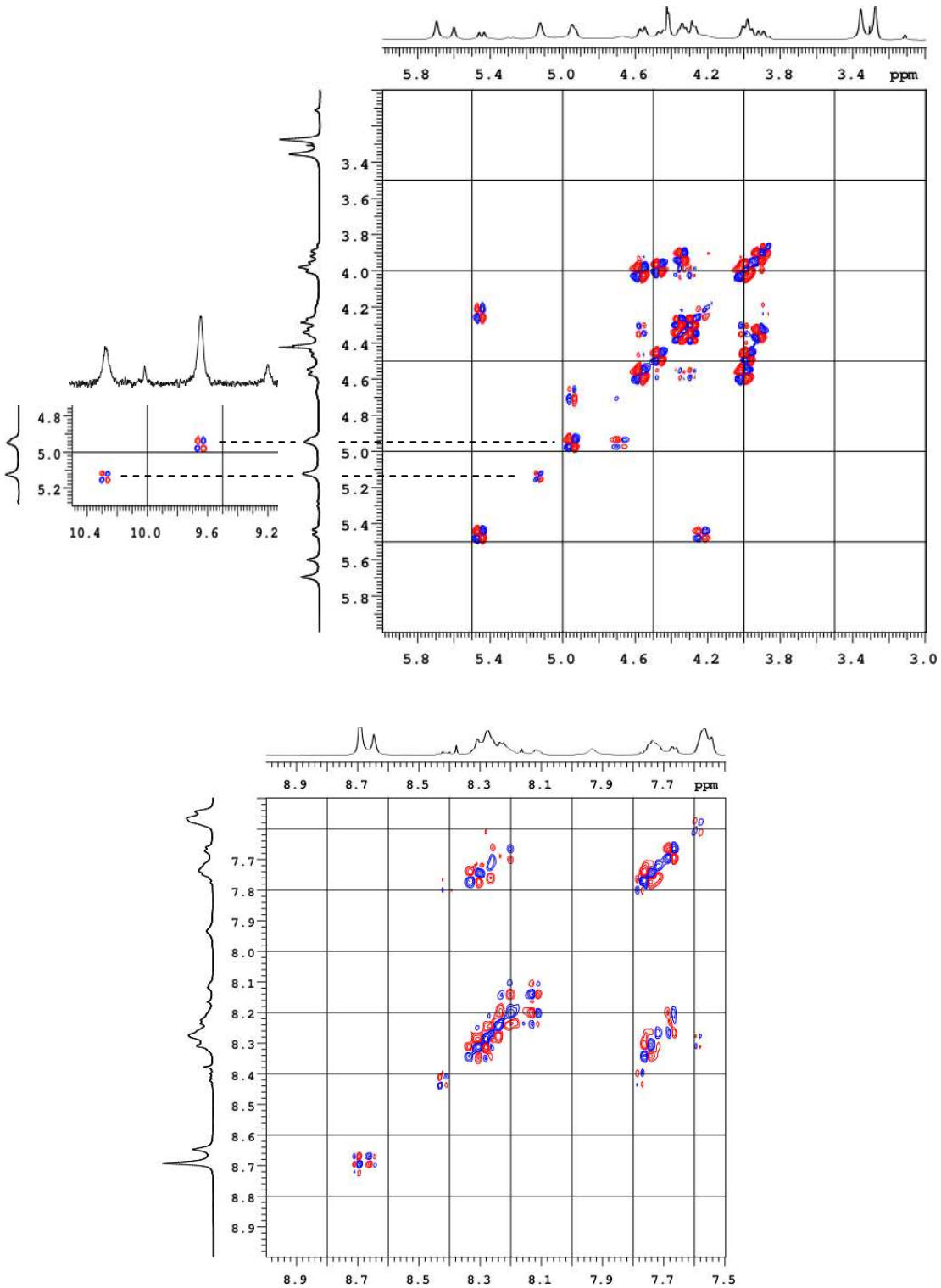

Figure S8: Regions of the dqfCOSY spectrum recorded at -35°C for a freshly prepared sample of [**3**·**H**$^+$**,NO$_3$]** (600 MHz, acetone-d_6).

The EXSY correlations observed in the 2D-ROESY spectrum (Figure S9) were used to identify the signals pertaining to the same chemical group in the three conformations. They reveal the two set of aromatic signals, referred to as ArHa and ArHb, for the calixarene core (Figure S10); these signals were clearly evidenced by 1D-ROESY experiments (Figure S11). The HMBC spectrum indicates that the ArHa signals belong to p-nitroanisol units (Figure S12). Indeed, ArHa and OMe ^{1}H signals are correlated to the same quaternary aromatic ^{13}C observed at about 162 ppm.

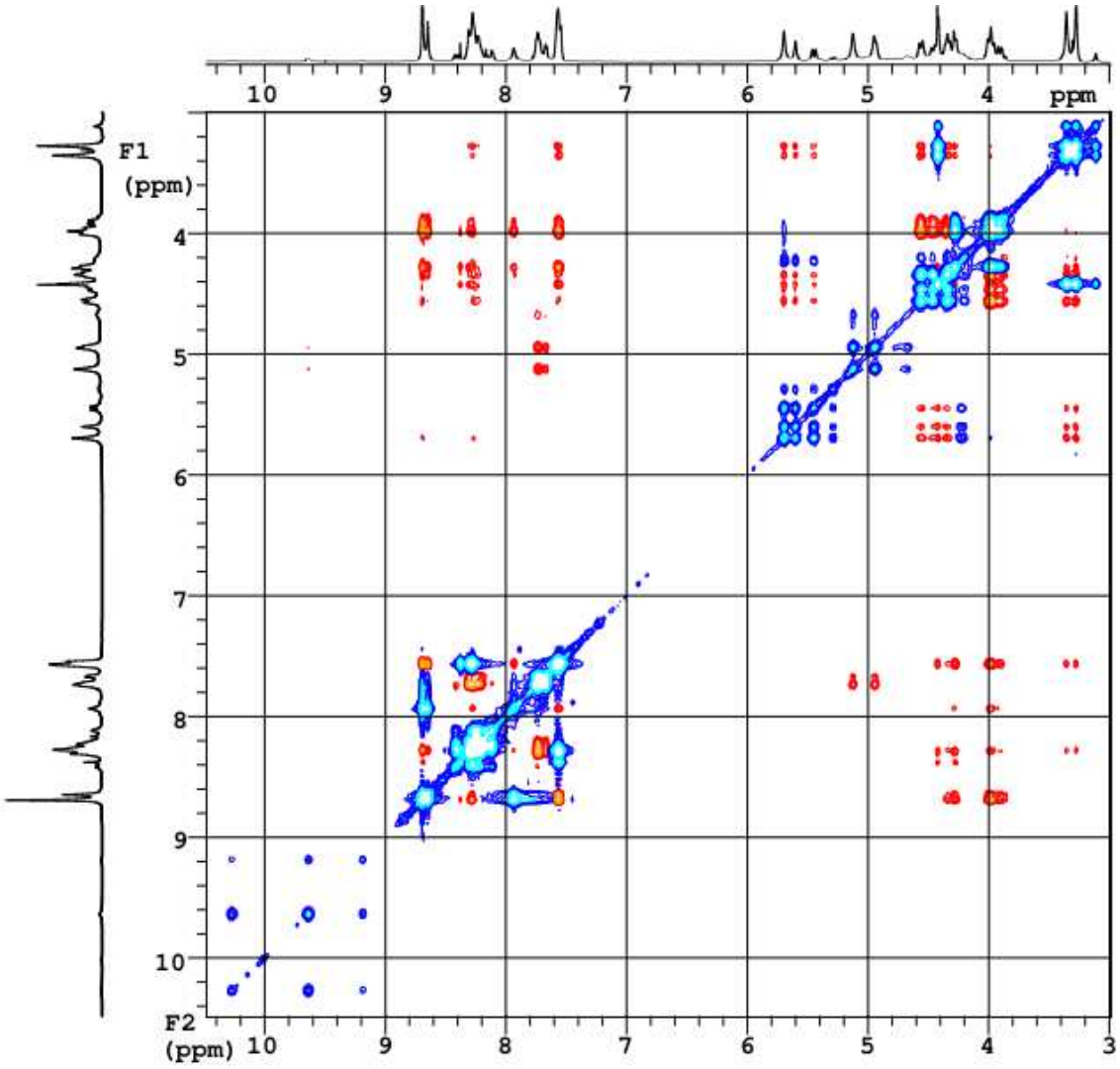

Figure S9: 2D-ROESY NMR spectrum of a freshly prepared sample of **[3·H^{+},NO$_3$]** recorded at -35°C (τ_{mix} = 500 ms, 600 MHz, acetone-d_6). Correlations due to chemical exchange (EXSY-type) are shown in blue; correlations arising from nuclear Overhauser effects (NOE-type) are in red.

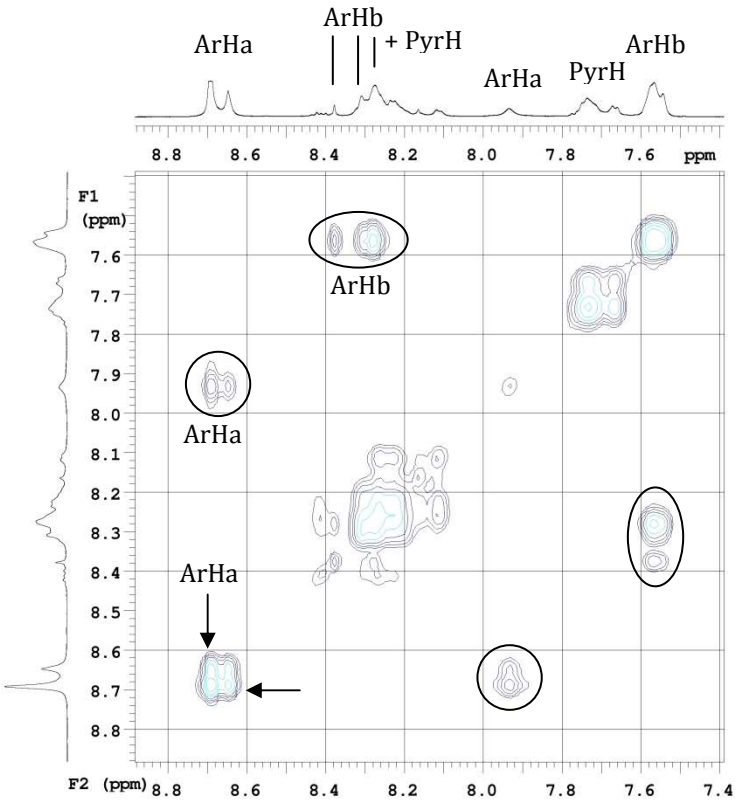

Figure S10: EXSY correlations observed in the aromatic region of the 2D-ROESY NMR spectrum of **[3·H$^+$,NO$_3$]** recorded at -35°C (τ_{mix} = 500 ms, 600 MHz, acetone-d_6). PyrH = ^{1}H of the pyridine moieties.

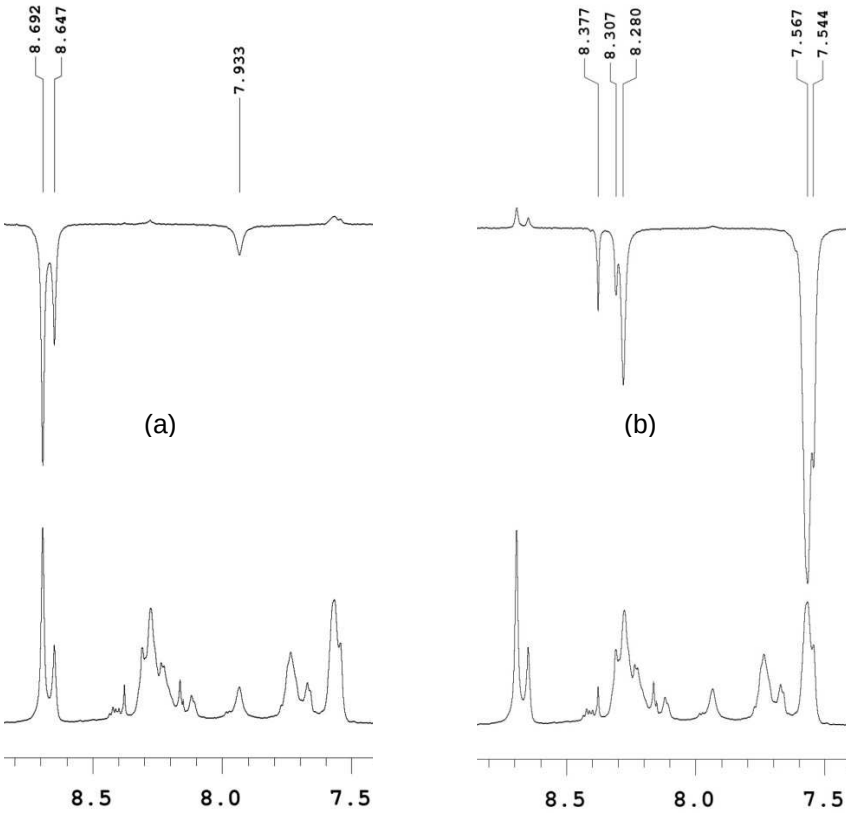

Figure S11: Aromatic region of 1D-ROESY spectra of [**3**·H^+,NO_3] recorded at -35°C (a) with selective excitation of the ArHa signals at 8.6-8.7 ppm and (b) with selective excitation of the ArHb signals at 7.5-7.6 ppm (τ_{mix} = 600 ms, 600 MHz, acetone-d_6).

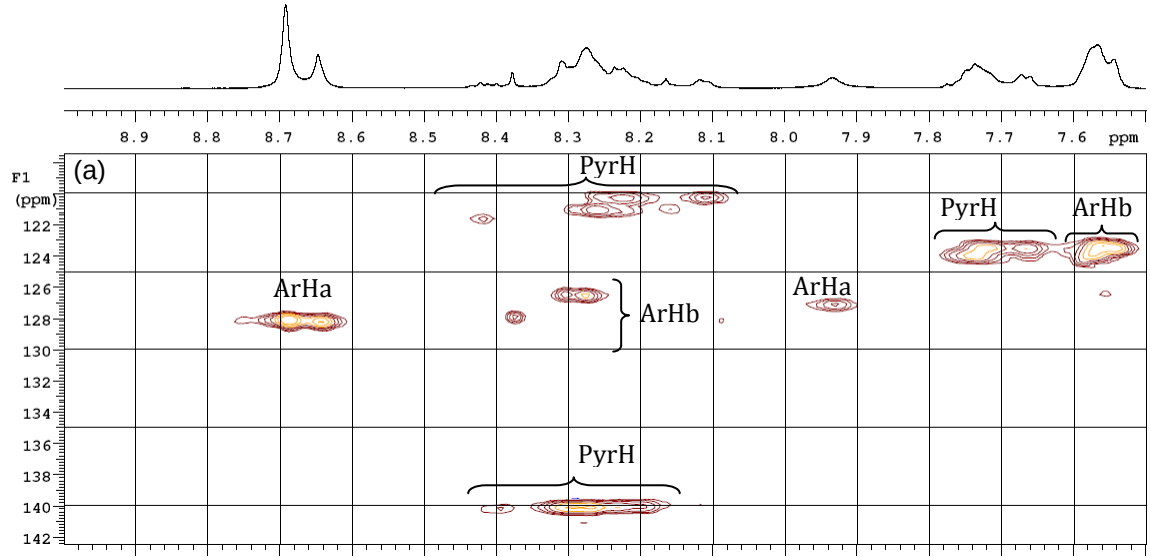

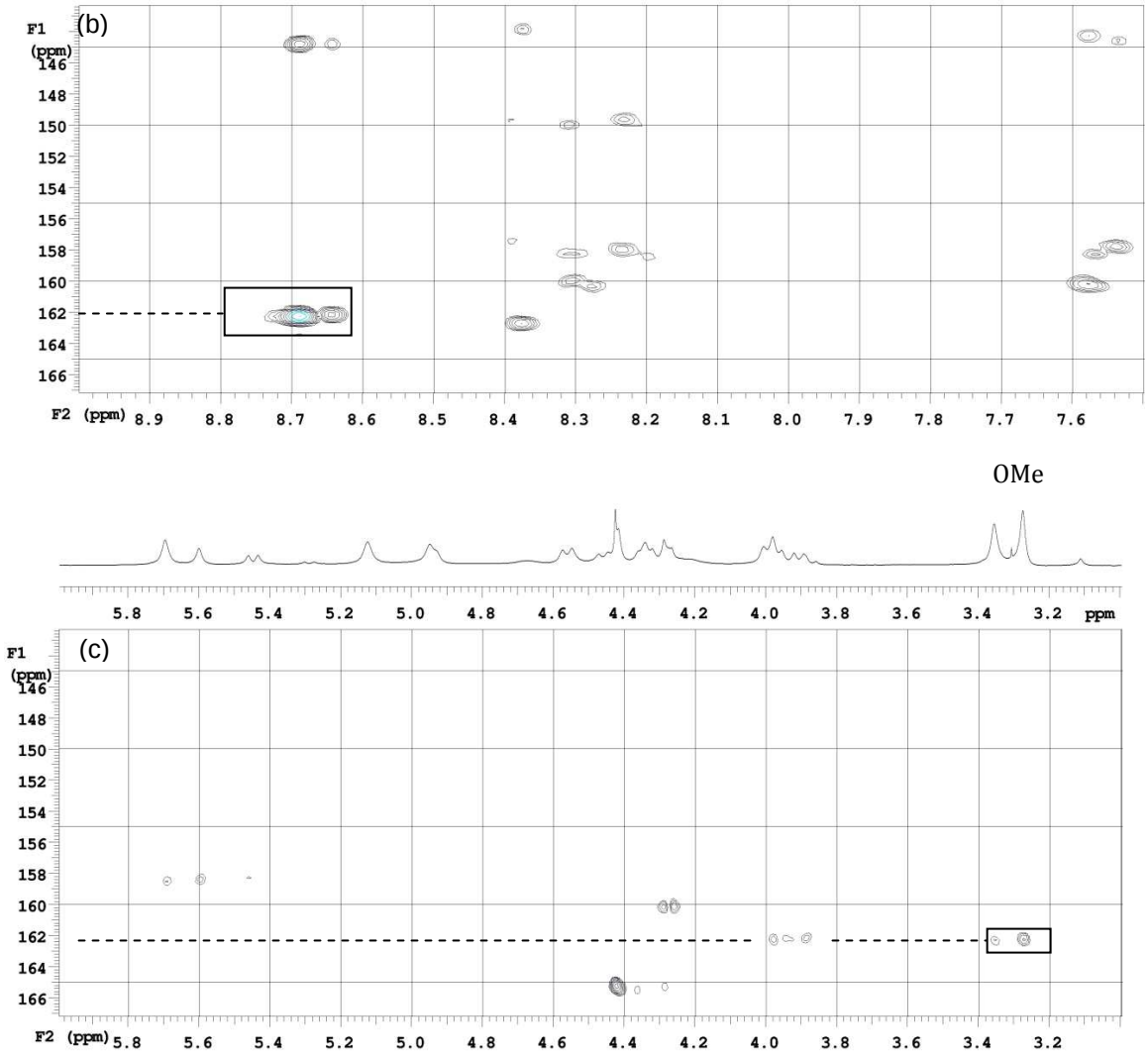

Figure S12: (a) Aromatic Region of the HSQC spectrum and (b,c) regions of the HMBC 8 Hz spectrum of [**3**·$\mathbf{H^+}$,$\mathbf{NO_3}$] recorded at -35°C (600 MHz, acetone-d_6) ; see Figure S14 for the HSQC correlations identifying the OMe signals.

In the aliphatic region of the ROESY-2D spectrum (Figure S13), the EXSY correlations clearly reveal two OMe signals at about 4.4 ppm (downfield shifted by more than 1 ppm) and one OCH_2 signal at about 4.2 ppm (upfield shifted by more than 1 ppm). These assignments are confirmed by the HSQC spectrum (Figure S14). The HSQC spectrum also reveals $ArCH_2$ groups characterized by a small ^1H diastereotopic shift ($\Delta\delta < 0.1$ ppm) with the corresponding ^{13}C signal downfield shifted by more than 5 ppm. This strongly suggests the occurrence of *anti* relative orientations of adjacent aromatic units, *i.e.* up-side-down inversion of at least one unit.[1]

As could have been expected, selective excitation of ArHa (^1H of the p-nitroanisol units) does not give rise to significant Overhauser effects with the OMe ^1H (Figure S15, see also the 2D-ROESY shown in Figure S9). In contrast, selective excitation of ArHb (^1H of the aromatic units bearing the TMPA cap) does yield such effects, which is consistent with the up-side-down inversion of (at least) one p-nitroanisol unit.

[1] a) Kanamathareddy *et al. J. Org. Chem.* **1994**, *59*, 3871-3879 ; b) Neri *et al. J. Am. Chem. Soc.* **1992**, *114*, 7814-7821

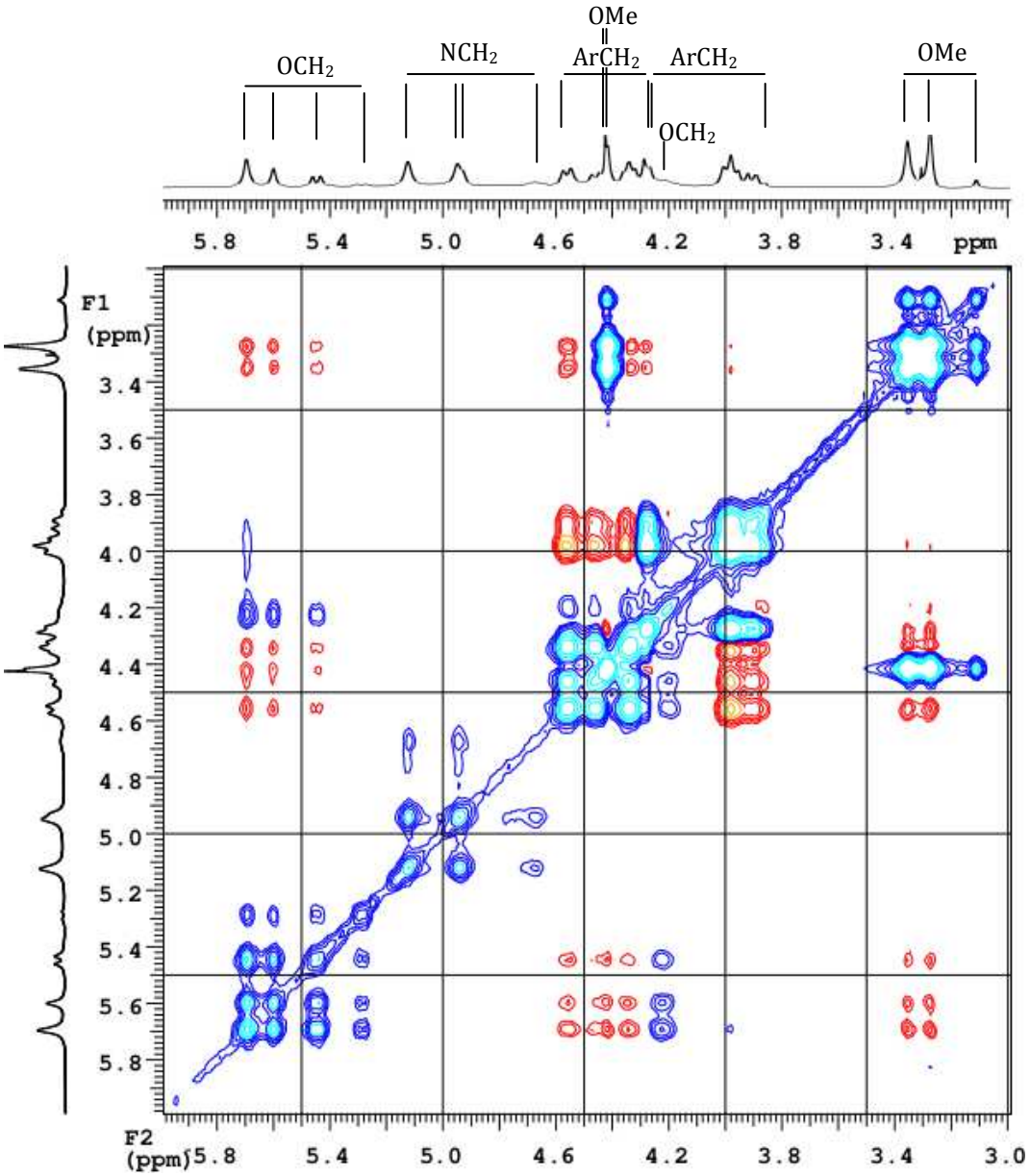

Figure S13: Aliphatic region of the 2D-ROESY NMR spectrum of [**3**·H^+,NO_3] recorded at -35°C (τ_{mix} = 500 ms, 600 MHz, acetone-d_6).

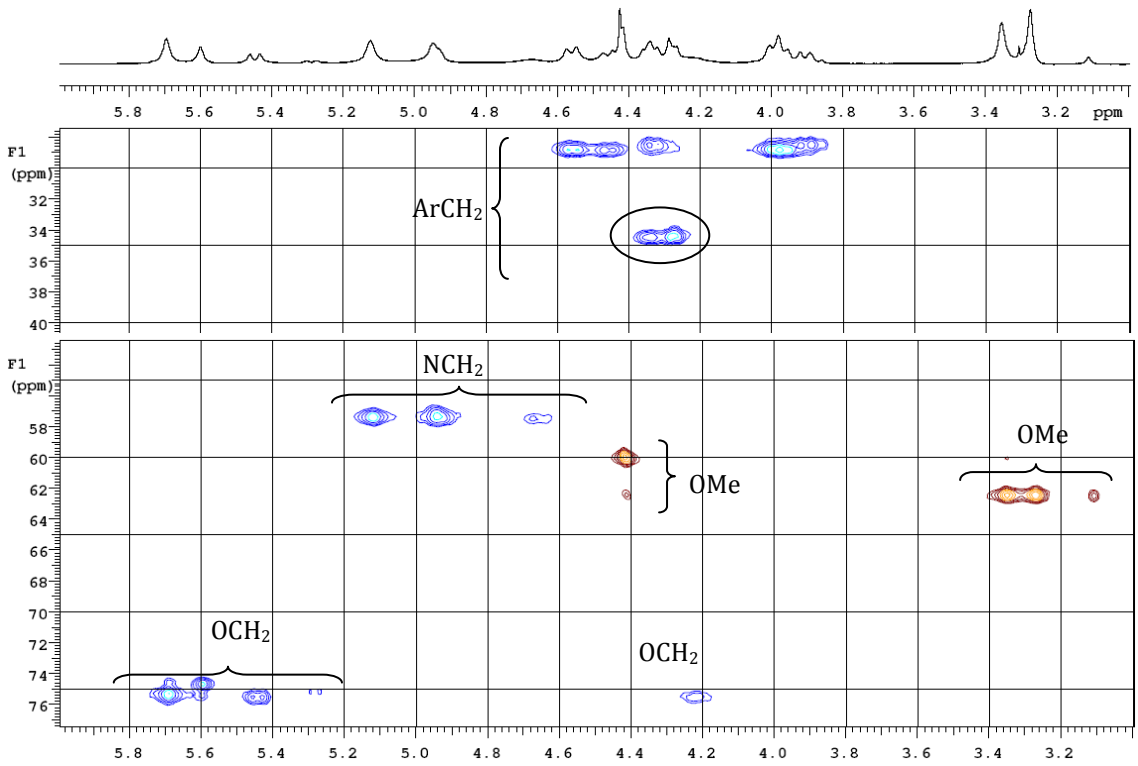

Figure S14: Aliphatic region of the edited-HSQC spectrum of **[3·H$^+$,NO$_3$]** recorded at -35°C (600 MHz, acetone-d_6).

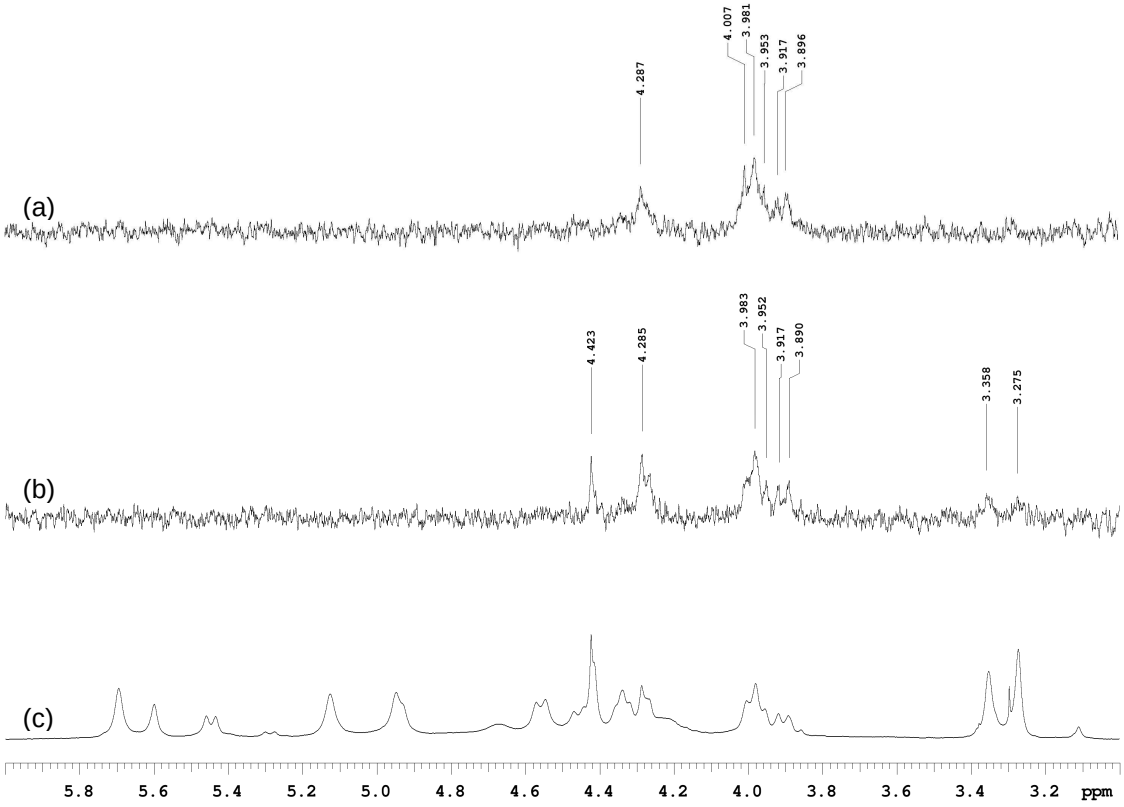

Figure S15: (a) Aliphatic region of 1D-ROESY spectra (τ_{mix} = 600 ms) of [**3**·**H**$^+$,**NO$_3$**] recorded at -35°C (a) with selective excitation of the ArHa signals at 8.6-8.7 ppm and (b) with selective excitation of the ArHb signals at 7.5-7.6 ppm; (c) corresponding region of the T_2-fitltered spectrum (600 MHz, acetone-d_6).

Deconvolution analysis of the ^{1}H NMR spectrum of [3·H$^+$,NO$_3$]

Figure S16 shows a deconvolution analysis of the NH$^+$ region of the ^{1}H NMR spectrum recorded at -35°. The model consists of a constant baseline and a single Lorenztian function for each signal (unresolved scalar couplings with the vicinal NCH_2 groups were ignored). By this way, the molar proportions of the three conformations were found to be:

I (53.9 ± 1.1) %,
II (33.4 ± 0.9) %,
III (12.7 ± 0.6) %.

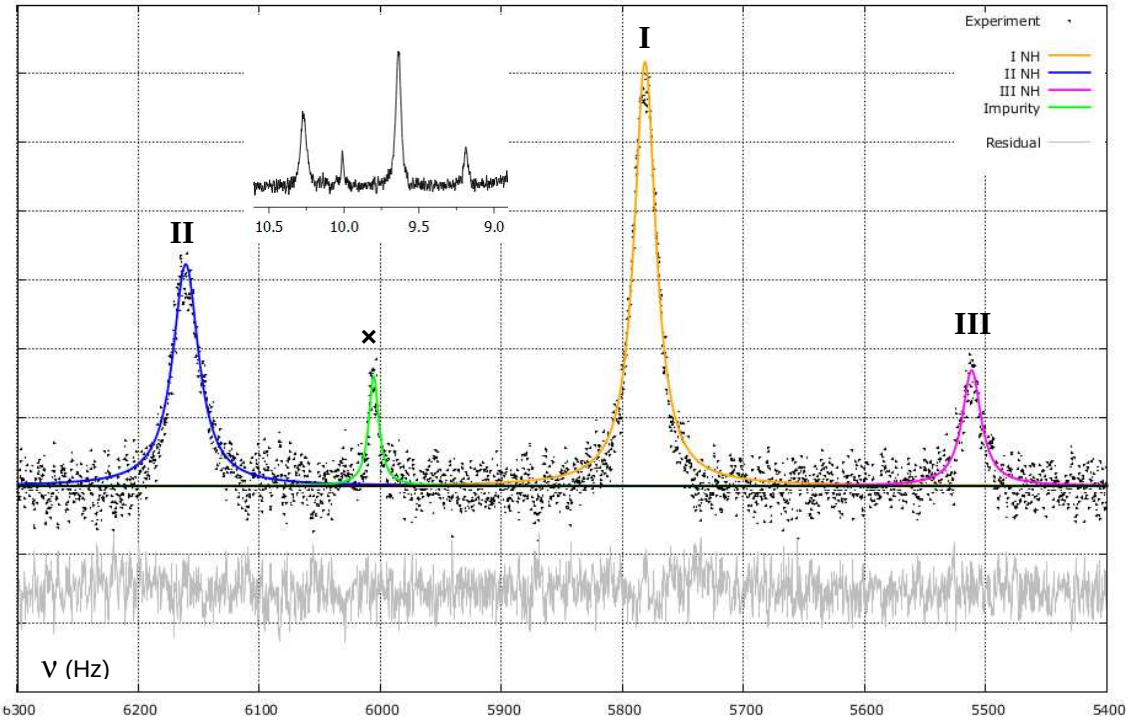

Figure S16: Deconvolution analysis of the NH$^+$ region of the ^{1}H NMR spectrum recorded at -35°C for a freshly prepared sample of **[3·H$^+$,NO$_3$]** (600 MHz, acetone-d_6). × = impurity. The residuals are shown under the scale.

A deconvolution analysis was also completed for the aliphatic region (Figure S17). The model consists of a constant baseline, a single Lorenztian function for each singlet signal, among which the broad signal of water, and two Lorenztian functions of identical intensity and identical linewidth for each doublet signal. For each conformation, the integrated intensities were constrained according to the number of ^{1}H and following assignment:

I corresponds to the partial cone conformation (C_s symmetrical),
II corresponds to the flattened-cone conformation (C_{3v} symmetrical),
III corresponds to the 1,3-alternate conformation (C_s symmetrical).

The scalar coupling constant of the doublets that are correlated in the dqfCOSY spectrum was constrained to the same value. The region between 4.4 and 4.1 ppm was discarded because it exhibits second order doublets and important signal overlapping.
This analysis properly accounts for the experimental spectrum and yields molar proportions in excellent agreement with the results obtained by the analysis of the NH^+ region:

I (53.8 ± 0.4) %,
II (33.2 ± 0.2) %,
III (13.0 ± 0.2) %.

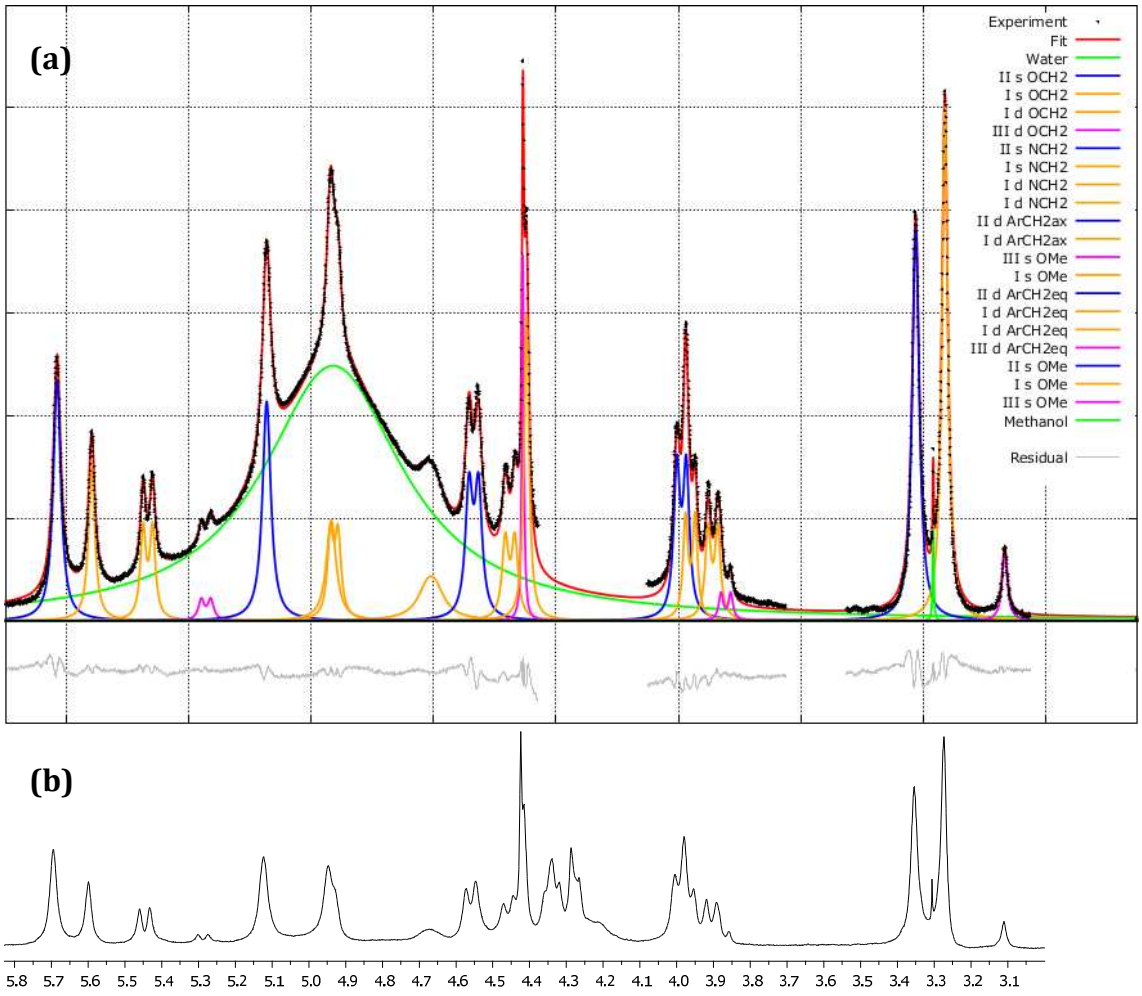

Figure S17: (a) Deconvolution analysis of the aliphatic region of the ^{1}H NMR spectrum recorded at -35°C for a freshly prepared sample of **[3·H$^+$,NO$_3$]**, the residuals are shown under the scale, and (b) corresponding T_2-filtered spectrum (600 MHz, acetone-d_6).

Flattened-cone conformation (II, C_{3v} symmetrical, 33% mole):

5.70 ppm, 6 H, s	OCH_2
5.12 ppm, 6 H, s	NCH_2
4.56 ppm, 6 H, d (J=15.4 Hz)	$ArCH_2$ (axial H)
3.99 ppm, 6 H, d (J=15.4 Hz)	$ArCH_2$ (equatorial H)

3.35 ppm, 9 H, s	OMe

Partial cone conformation (I, C_s symmetrical, 54% mole):

5.60 ppm, 2 H, s	OCH_2
5.45 ppm, 2 H, d (J=15.4 Hz)	OCH_2
4.95 ppm, 2 H, s	NCH_2
4.94 ppm, 2 H, d (J=12.3 Hz)	NCH_2
4.67 ppm, 2 H, d (J=12.3 Hz)	NCH_2
4.46 ppm, 2 H, d (J=15.4 Hz)	$ArCH_2$ (axial H)
4.41 ppm, 3 H, s	OMe (reversed p-nitroanisol unit)
3.97 ppm, 2 H, d (J=15.4 Hz)	$ArCH_2$ (equatorial H)
3.91 ppm, 2 H, d (J=15.8 Hz)	$ArCH_2$ (equatorial H)
3.27 ppm, 6 H, s	OMe

1,3-alternate conformation (III, C_s symmetrical, 13% mole):

5.29 ppm, 2 H, d (J=15.4 Hz)	OCH_2
4.42 ppm, 6 H, s	OMe (reversed p-nitroanisol units)
3.87 ppm, 2 H, d (J=15.9 Hz)	$ArCH_2$ (equatorial H)
3.11 ppm, 3 H, s	OMe

Van't Hoff plot for the conformational equilibria of [3·H$^+$,NO$_3$]

^{1}H NMR spectra of [**3·H$^+$,NO$_3$]** recorded at variable temperature, down to -70°C, 5 days after sample dissolution are shown in Figure S18. As a consequence of H→D exchange with acetone-d_6, the intensity of the signal of water as well as the intensity of the NH$^+$ signals (not shown) are much weaker. The signals do no exhibit significant chemical shift variation with temperature. In contrast, both the relative integrated intensity and the linewidth do. Deconvolution analysis of the aliphatic region of these spectra was completed using the same model as described above. The molar proportions of the three conformations are shown in Figure S19a as a function of temperature. The corresponding van 't Hoff plots are given in Figure S19b.

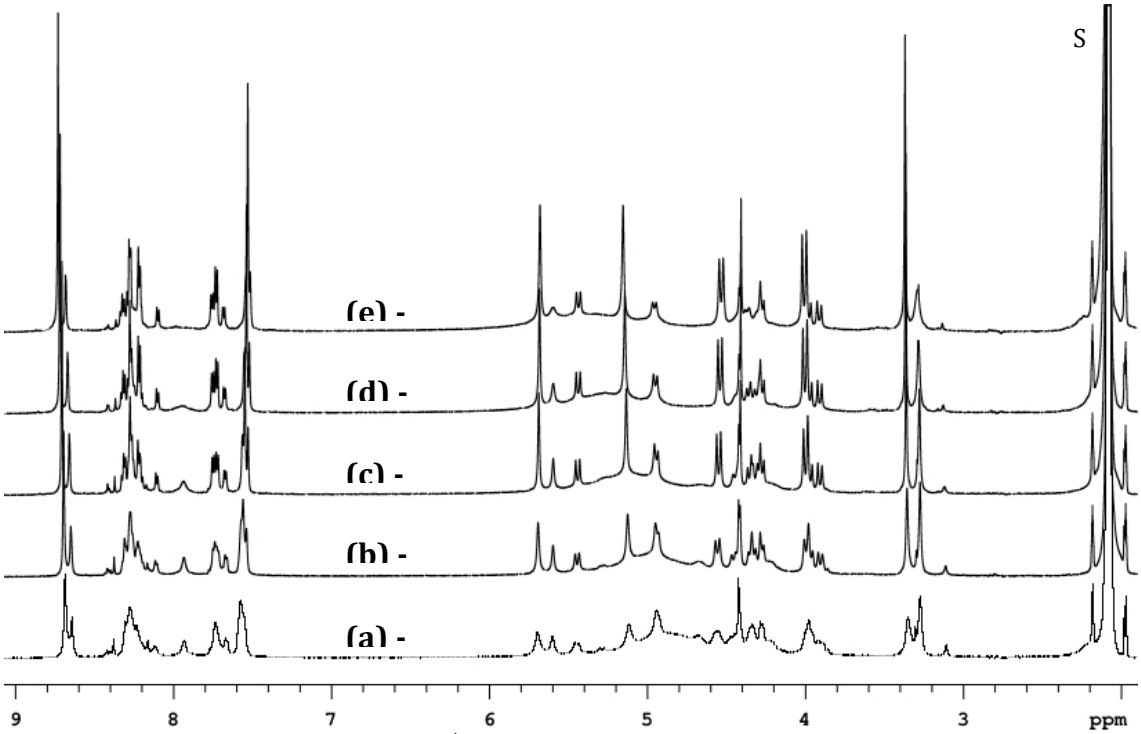

Figure S18: Variable temperature ^{1}H NMR spectra of a sample of [**3·H$^+$,NO$_3$]** recorded 5 days after sample dissolution (600 MHz, acetone-d_6). S=solvent.

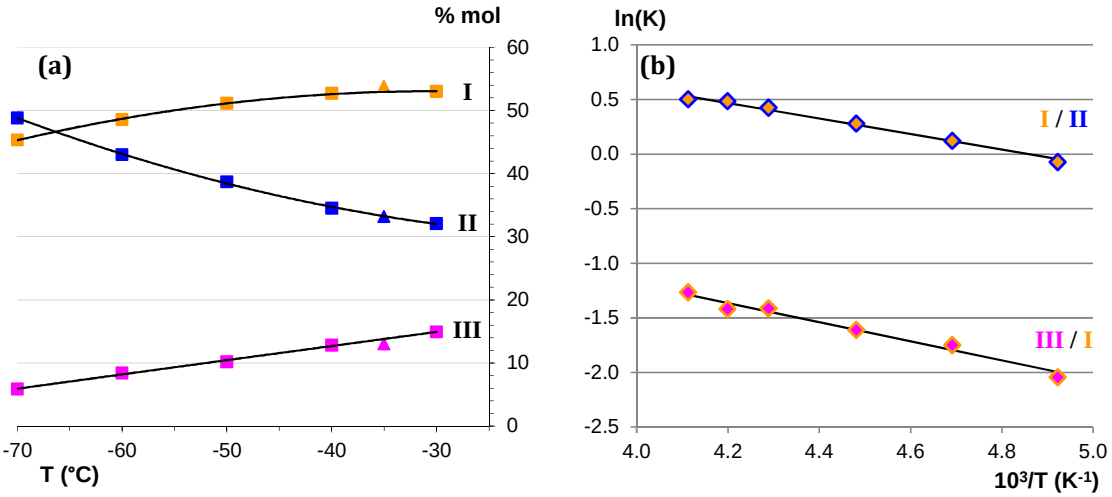

Figure S19: (a) Molar proportions of the three conformations of **[3·H$^+$,NO$_3$]** as determined by deconvolution of the aliphatic region of variable temperature ^{1}H NMR spectra (600 MHz, acetone-d_6) and (b) corresponding van 't Hoff plot for the ratios I / II and III / I. In (a), the triangles are the results for the freshly prepared sample and the lines are guides for the eyes.

The thermodynamic parameters estimated for the inversion of one p-nitroanisol unit, i.e. for the II (C_{3v}) $\rightleftharpoons$ I (C_s) equilibrium, are $\Delta H°$= +(5.9 ± 0.6) kJ mol^{-1} and $\Delta S°$= +(29 ± 3) J K^{-1} mol^{-1}. For the second inversion, i.e. for the I (C_s) $\rightleftharpoons$ III (C_s) equilibrium, they were estimated to be $\Delta H°$= +(7.3 ± 0.6) kJ mol^{-1} and $\Delta S°$= +(19 ± 3) J K^{-1} mol^{-1}. The errors corresponds to the standard deviation determined from the analysis of 100 pseudo-experimental data sets obtained by adding random errors generated from Gaussian distributions and using an absolute standard error of ± 0.1 K on the temperature and a relative standard error of ± 10 % on the equilibrium constant (on the molar ratio).

The full width at half-height of various ^{1}H NMR signals of the two principal conformations of **[3·H$^+$,NO$_3$]** are shown in Figure S20 as a function of temperature. For the flattened-cone conformation, the linewidth of the OCH_2, NCH_2 and OMe signals are similar, it decreases for decreasing temperatures and the variation is globally monotonous, as expected. In contrast, some signals of the partial cone conformation are significantly broader and, at low temperature, the linewidth increases for decreasing temperatures. Interestingly, the linewidth of the OMe signal observed at about 4.41 ppm, which belongs to the up-side-down p-nitroanisol unit, exhibits the expected temperature variation. These observations suggests that an additional dynamic process affecting the TMPA cap occurs and that this process is more hindered in the partial cone conformation.

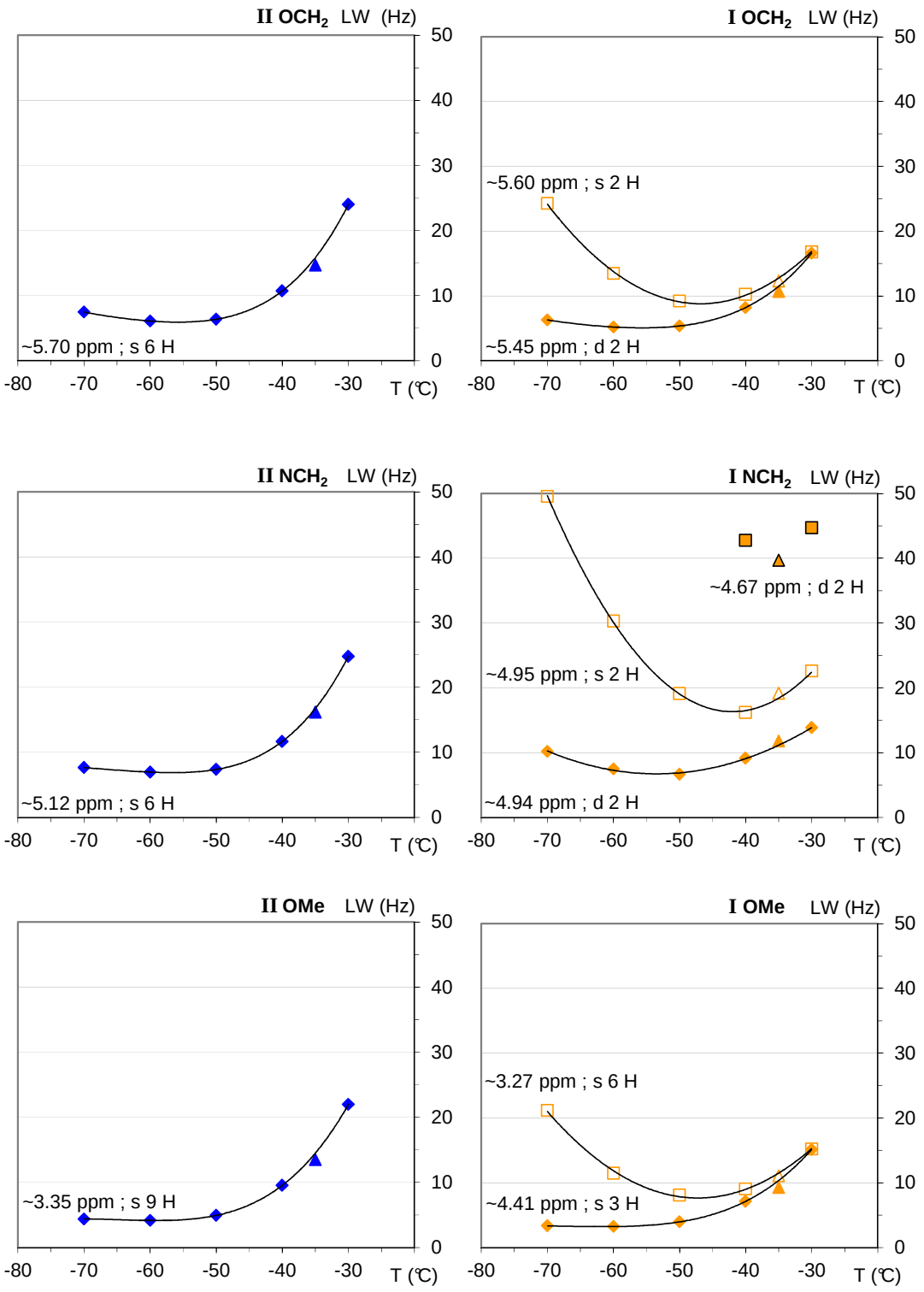

Figure S20: Full width at half-height (LW) of various ^{1}H NMR signals of **[3·H^{+},NO$_3$]** as determined by deconvolution of the aliphatic region of variable temperature spectra (600 MHz, acetone-d_6). Left side: data for the flattened-cone conformation II. Right side: data for the partial cone conformation I. The triangles are the results for the freshly prepared sample; the lines are guides for the eyes.

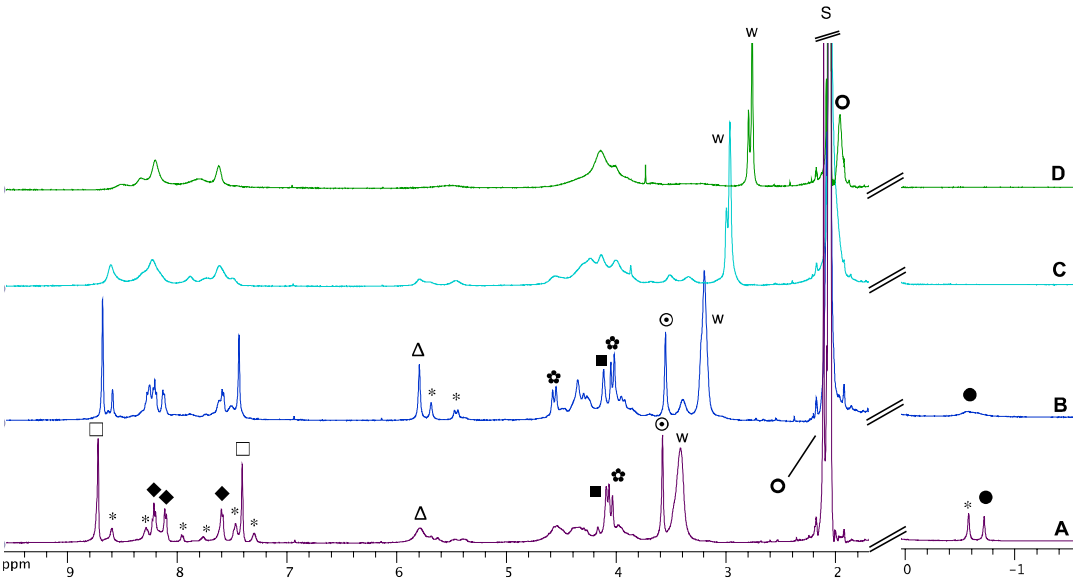

Figure S21: ^{1}H NMR (500 MHz, acetone-d^6) of **[Cu^{I}3(CH$_3$CN)]B(C$_6$F$_5$)$_4$**: A) 240K; B) 260K; C) 280K; D) 300K. □=H_{Ar}, ◆=H_{Py}, w=water, Δ=OCH_2, ■=NCH_2, ✿=$ArCH_2$, ⊙=OCH_3, S=solvent, O=CH_3CN_{out}, ● =CH_3CN_{in}, *=less symmetrical conformation.

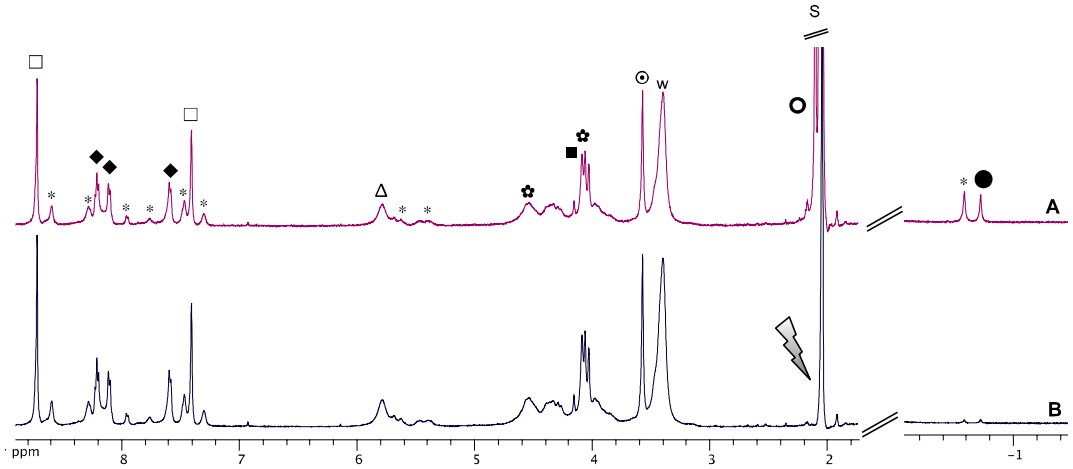

Figure S22: Transfer Saturation experiment (t= 2s, power of irradiation= 50dB) on the ^{1}H NMR (500 MHz, acetone-d^6, 240K) of **[Cu^{I}3(CH$_3$CN)]B(C$_6$F$_5$)$_4$**: A) irradiation at 15ppm; B) irradiation at 2.13 ppm (resonance of CH_3CN_{out}). □=H_{Ar}, ◆=H_{Py}, w=water, Δ=OCH_2, ■=NCH_2, ✿=$ArCH_2$, ⊙=OCH_3, S=solvent, O=CH_3CN_{out}, ● =CH_3CN_{in}, *=less symmetrical conformation.

Deconvolution analysis of the ^{1}H NMR spectrum of [Cu^{I}3(CH$_3$CN)]B(C$_6$F$_5$)$_4$.

A deconvolution analysis was completed for selected aliphatic signals of the ^{1}H NMR spectrum recorded at 260 K (Figure S23). It yields the following molar proportions:

partial cone conformation: (47.3 ± 1.6) %,
flattened-cone conformation: (41.1 ± 1.1) %,
1,3-alternate conformation: (11.6 ± 1.7) %.

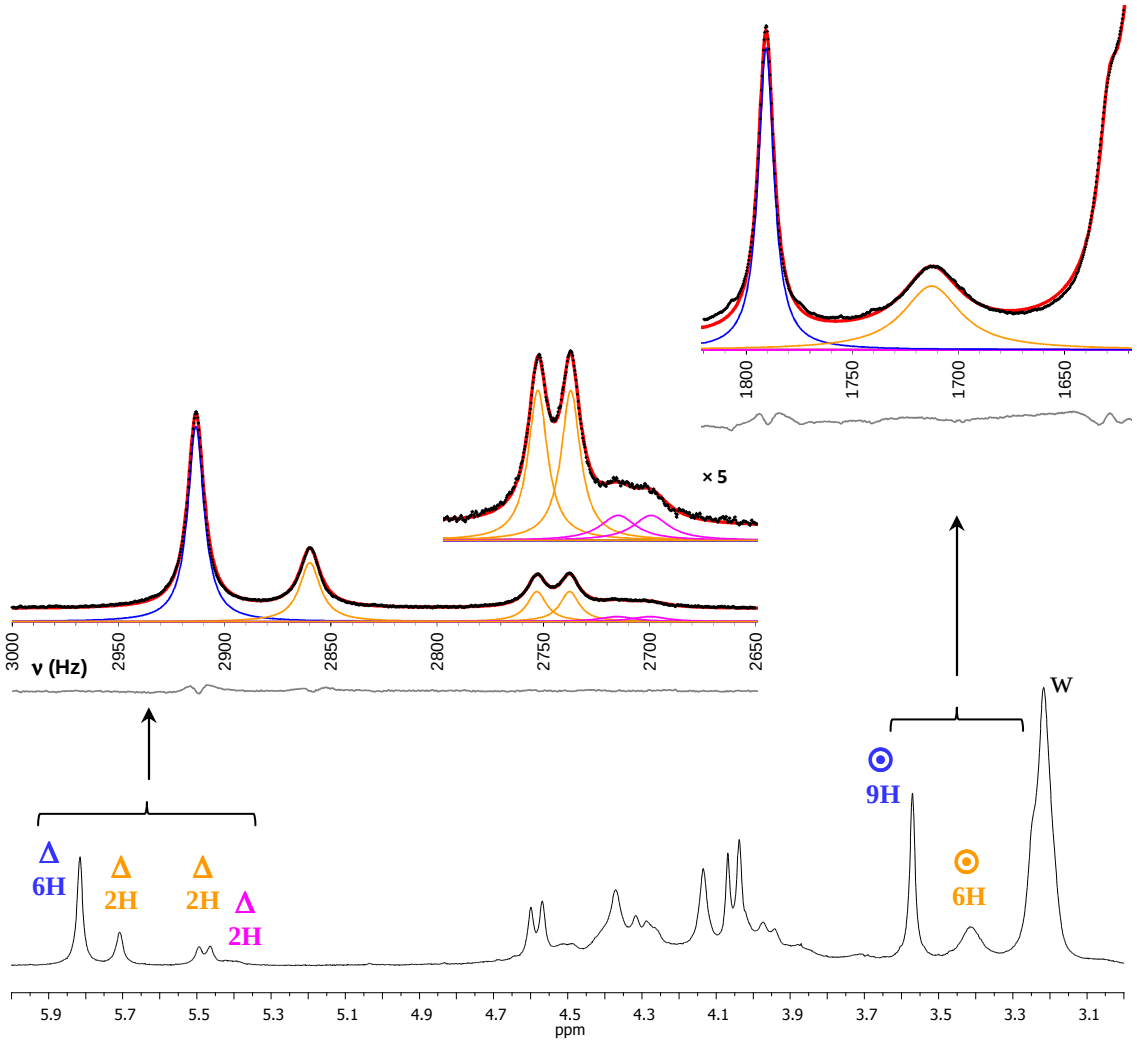

Figure S23: Deconvolution analysis of selected ^{1}H NMR signals of **[Cu^{I}3(CH$_3$CN)]B(C$_6$F$_5$)$_4$** (260 K, 500 MHz, acetone-d_6). w=water, Δ=OCH$_2$, ⊙=OCH$_3$. The residuals are shown under the scales.

Flattened-cone conformation (C_{3v} symmetrical):

5.83 ppm, 6 H, s	OCH$_2$	linewidth = 9.2 Hz
3.58 ppm, 9 H, s	OMe	linewidth = 8.9 Hz

Partial cone conformation (C_s symmetrical):

5.72 ppm, 2 H, s	OCH$_2$	linewidth = 11.7 Hz
5.49 ppm, 2 H, d (J=15.4 Hz)	OCH$_2$	linewidth = 15.4 Hz

3.42 ppm, 6 H, s OMe linewidth = 32.4 Hz

1,3-alternate conformation (C_s symmetrical):

5.41 ppm, 2 H, d (J=15.4 Hz) OCH_2 linewidth = 15.5 Hz

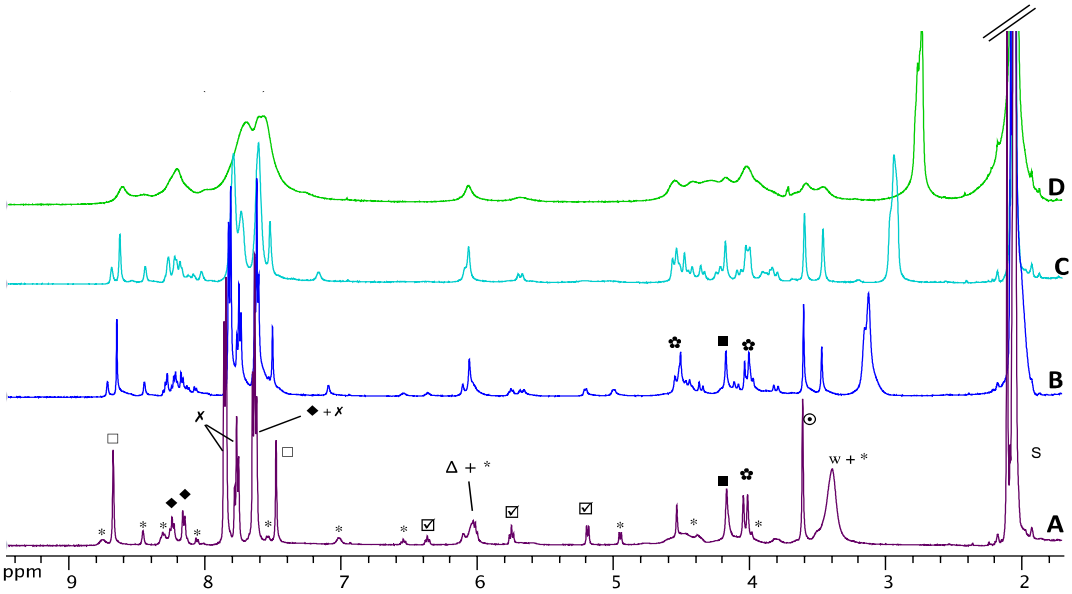

Figure S24: ^{1}H NMR (500 MHz, acetone-d^6) of **[Cu^{I}3(PhCN)]B(C_6F_5)$_4$**: A) 240K; B) 260K; C) 280K; D) 300K. □=H_{Ar}, ◆=H_{Py}, ✗=$PhCN_{out}$, Δ=OCH_2, ☑=$PhCN_{in}$, ■=NCH_2, ✿=$ArCH_2$, w=water, ⊙=OCH_3, S=solvent, *=less symmetrical conformation.

XRD structure of [$3H^+$, NO_3^-]

Upon standing to air, out of their mother liquor, the crystals are destroyed within a minute and loose their diffraction properties. They were directly fished out from the crystallisation medium using a Hampton® cryoloop and immediately quenched on the goniometer in a nitrogen stream at 100 K. The data collection consists of 120 frames of 4° exposure each. Two crystals randomly oriented were used independently. Diffraction data were separately integrated using the XDS package[2] and merged with the CCP4 suite of programs.[3] A single file of structure factors was produced for determining and refining the structure.[4] Data statistics are given in Table S1.

Table S1 **[$3H^+$, NO_3^-]** - Data statistics - Recordings

System:	Monoclinic
Space group:	$P2_1/c$
Parameters: a = b = c = b = Z =	 15.502(1) Å 13.181(1) Å 40.203(1) Å 96.52(3) ° 4
Resolution limits: (Å) * (highest shell in parentheses)	10 – 0.922 (1.1 – 0.922)
No of recorded reflections	51 365 (4 520)
No of independent reflections	8 227 (1897)
No of observed reflections Criteria: $I \geq 4s(I)$	8173 (1153)
Rsym (%)	4.65 (10.9)
Redondency	6.1 (3.5)
Completeness:	10 – 1.1 Å: 98.7 % (1.1 – 0.922: 42.4 %)

* The practical resolution is limited to 1.05 Å due to detector geometry limitations (the central circular zone). The maximum resolution of 0.922 Å corresponds to the detector edges.

The structure was solved using the SHELXD program (Sheldrick, 2008),[4] a correct solution was found in the first 100 trials. After location of the missing atoms by Fourier recycling, the starting model comprised in addition to the calix[6] ligand, one nitrate as counter ion, plus four acetone molecules - three of them with partial occupancies - and two water molecules hydrogen bonded to the nitrate. The acetone with occupancy equal to unity is located within the calix[6] cone; the others are distributed in the packing.

The refinements were conducted with the SHELXL program, first with isotropic then anisotropic thermal factors. Hydrogens were calculated at their theoretical places with an isotropic thermal factor riding on that of the bonded atom. The acetone molecule hosted in the calix cone was refined with an occupancy factor equal to unity but it was clear that

[2] Kabsch, W. *Acta Cryst.* **2010**, *D66*, 125-132.
[3] CCP4 *Acta Cryst.* **1994,** *D50*, 760-763.
[4] Sheldrick, G. M. *Acta Cryst.* **2008,** *A64*, 112-122.

the three other sites distributed within the packing have lower occupancies. They were refined independently (see Table S2). As to achieve reasonable geometries, restraints on distances (bonds and angles) as well as planar restraints were applied to all acetones. The resulting coordinate data were deposited with the Cambridge Crystallographic Data Centre 12, Union Road, CB2 1EZ Cambridge, UK. They are available upon request to http://www.ccdc.cam.ac.uk/.

Table S2 – Refinement of the **[$3H^+$, NO_3^-]** crystal structure

Formula	$C_{66}H_{54}N_{10}O_{18}^+$, NO_3^-, 2.7(C_3H_60), 2 H_2O ,
Mw	1509.46
No of non-H atoms refined	116
Refined occupancy factors of the 3 acetone molecules in the packing	0.480 – 0.621 – 0.589
No of refined parameters	1018
No of restraints used (dist. and planes)	102
No of structure factors (*Fo*) used	8227
No of observed *Fo*'s (with *Fo* > 4s(*Fo*)	8173
R factor (on obs. *Fo*)	0.077
R factor (all data)	0.078
Rw factor (on obs. Fo^2)	0.194
Rw factor (all Fo^2 data)	0.195
Min/max in last Fourier difference map	-0.50 / +0.26 $e^-/Å^3$
Deposition code with the CCDC	985920

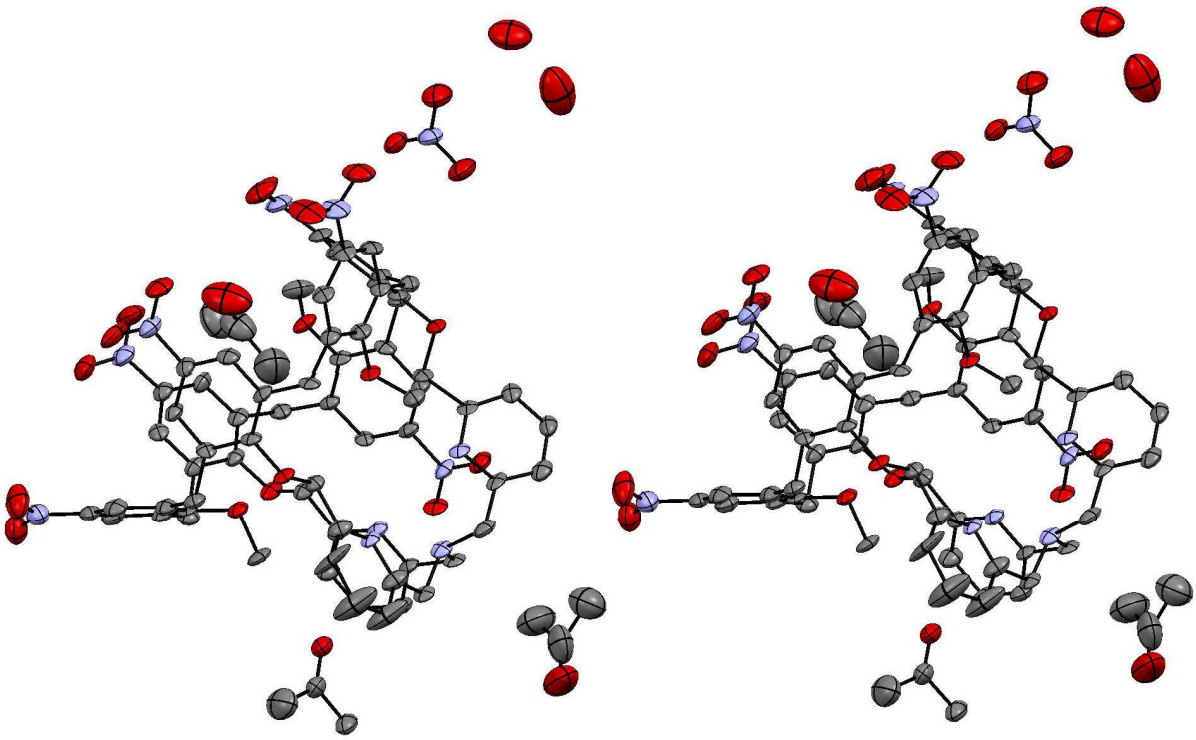

Figure S25: Stereo view of the asymmetric unit content in ORTEP-like representation (ellipsoids at the 50 % level of density probability)